Boron doped diamond as a low biofouling material in aquatic environments: Assessment of *Pseudomonas aeruginosa* biofilm formation

*Lee J. Simcox [1,2], Rui P. A. Pereira [3], Elizabeth M. H. Wellington [3], Julie V. Macpherson [1]**

[1] Department of Chemistry, University of Warwick, Coventry, CV4 7AL, United Kingdom

[2] Molecular Analytical Science Centre for Doctoral Training, University of Warwick, Coventry, CV4 7AL, United Kingdom

[3] School of Life Sciences, University of Warwick, Coventry, CV4 7AL, United Kingdom

KEYWORDS. Diamond, boron doped diamond, biofilm, biofouling, *Pseudomonas aeruginosa*, sensor, roughness, hydrophobicity

ABSTRACT

Boron doped diamond (BDD), given the robustness of the material, is becoming an electrode of choice for applications which require long term electrochemical monitoring of analytes in aqueous environments. However, despite the extensive work in this area there are no studies which directly assess the biofilm formation (biofouling) capabilities of the material, which is an essential consideration since biofouling often causes deterioration in sensor performance. *Pseudomonas aeruginosa* is one of the most prevalent bacterial pathogens linked to water-related diseases, with a strong capacity for forming biofilms on surfaces that are exposed to

aquatic environments. In this study we comparatively evaluate the biofouling capabilities of oxygen-terminated (O-)BDD against materials commonly employed as either the packaging or sensing element in water quality sensors, with an aim to identify factors which control biofilm formation on BDD. We assess biofilm formation of *P. aeruginosa* monospecies in two different growth media, Luria-Bertani, a high nutrient source and drinking water, a low nutrient source, at two different temperatures (20 °C and 37 °C). Biofilm formation from multispecies bacteria is also investigated. The performance of O-BDD, when tested against all other materials, promotes the lowest extent of *P. aeruginosa* monospecies biofilm formation, even with corrections made for total surface area (roughness). Importantly, O-BDD shows the lowest water contact angle of all materials tested, *i.e.* greatest hydrophilicity, strongly suggesting that for these bacterial species, the factors controlling the hydrophilicity of the surface are important in reducing bacterial adhesion. This was further proven by keeping surface topography fixed and changing surface termination to hydrogen (H-), to produce a strongly hydrophobic surface. A noticeable increase in biofilm formation was found. Doping with boron also results in changes in hydrophobicity/hydrophilicity compared to the un-doped counterpart, which in turn affects bacterial growth. For practical electrochemical sensing applications in aquatic environments, this study highlights the extremely beneficial effects of employing smooth, O-terminated (hydrophilic) BDD electrodes.

INTRODUCTION

In aquatic environments there is a critical need to monitor water quality, analyzing parameters such as pH, dissolved gases, organic content, and heavy metals in order to fulfil quality control, environmental management, or regulatory compliance.[1] Monitoring typically involves the collection of discrete samples, followed by analysis in a laboratory or on-site if instrumentation permits.[2] The use of continuous *in situ* (or on-line) monitoring is considered most beneficial as it allows automatic, real-time measurements directly at the water source of interest.[1,2] However, one of the biggest challenges with *in situ* monitoring is deterioration of sensor performance over time due to biofouling, which provides a significant obstacle to obtaining reliable long-term measurements.[3–5] Biofouling is the accumulation of unwanted biological matter, and in aquatic environments this is often due to the formation of microbial biofilms.[6–8] Biofilms are complex and dynamic communities of microorganisms attached to a surface.[9] Once adhered, the bacteria proliferate, produce an extracellular polymeric matrix, and form a matured biofilm.[10,11] Biofilms are not only a problem for *in situ* sensing and analysis, but also for a wide variety of medical, environmental and industrial contexts.[6,7,10,12–16]

Given the negative implications of biofilm formation, there is a vast amount of research into strategies for the prevention of surface biofouling. These surface modifications range from the development of surface coatings and anti-bacterial adhesion agents, to the incorporation of silver or copper nanoparticles and antimicrobial agents, to engineering nanostructured materials.[17–22] However, for sensing applications, it is not always possible to modify the sensor surface without adversely affecting the performance properties. This is especially true of devices where the sensing element, *e.g.* an electrode, is directly exposed to the solution.

As a sensor material, in particular for *in situ* and on-line applications, boron doped diamond (BDD) is being actively explored as a result of the superior properties of the material, such as hardness, chemical inertness, and corrosion resistance.[23] BDD is typically operated as an

electrochemical sensor, packaged in either insulating undoped diamond[24] or a non-diamond material.[25] Undoped diamond is often claimed to be a low biofouling material,[26,27] however, the term biofouling is used loosely in the sensor literature and most biofouling studies investigate proteins[26] or neuronal cells.[28] However, these are not representative of a biofilm model of fouling, which is applicable under aquatic environmental conditions. Indeed, their mechanism of interaction is likely to be very different to that of a bacterial cell.[29] To date, there is no information on the interaction of bacterial cells with BDD, or indeed how doping may modify this interaction. Previous work focused only on the anti-adhesive properties of nanocrystalline diamond, which itself contains significant non-diamond sp^2 carbon impurities.[30–32]

In this study, we investigate for the first time the bacterial biofilm formation capabilities of both oxygen terminated (O-) and hydrogen terminated (H-) BDD, and identify the possible factors[33–38] which play a role in adherence of bacteria to these surfaces. Biofilm formation is examined in relation to other electrode or packaging materials, including undoped diamond, stainless steel, screen printed carbon (SPC), alumina, copper, and polyvinyl chloride (PVC). We focus on *Pseudomonas aeruginosa* (five bacterial strains) as it is regarded as one of the most prevalent opportunistic bacterial pathogens linked to water-related diseases,[16] is a strong biofilm producer, and is commonly detected in both natural and man-made water ecosystems.[11] As this species is often part of a multispecies bacterial biofilm community,[39] we also combine *P. aeruginosa* with other relevant biofilm-producing bacterial species widely present in water systems (*Acinetobacter baumannii*, *Aeromonas hydrophila*, *Klebsiella pneumoniae*, and *Staphylococcus aureus*).[40–42] The biofilm-forming properties of the materials are directly compared using a range of complementary techniques, including crystal violet (CV) dye staining, scanning electron microscopy (SEM), and confocal laser scanning microscopy (CLSM).[8,43]

EXPERIMENTAL SECTION

Substrates. Substrate materials employed for biofilm growth were: unplasticized PVC (Goodfellow Cambridge, Huntingdon, UK), AISI 304 stainless steel (Goodfellow Cambridge, Huntingdon, UK), copper (Goodfellow Cambridge, Huntingdon, UK), electrochemical processing grade BDD (polycrystalline and freestanding; Element Six, Didcot, UK), thermal grade intrinsic diamond (polycrystalline and freestanding; Element Six, Didcot, UK), alumina (CoorsTek, Fife, UK), and SPC (Gwent Electronic Materials, Pontypool, UK). The BDD is doped > 10^{20} B atoms cm^{-3}, which is above the metallic threshold.[23] All materials were cut to 4 mm diameter round discs using laser micromachining (E-355H-3-ATHI-O, Oxford Lasers, Didcot, UK), with the exception of copper and SPC, which were supplied pre-cut by the manufacturer. Diamond and BDD substrates were acid cleaned by exposure to a solution of 96% sulfuric acid (reagent grade; Sigma Aldrich, St. Louis, USA) saturated with potassium nitrate (reagent grade; Sigma Aldrich, St. Louis, USA) which was heated to a temperature of *ca*. 200 °C for 30 min; this process ensures that the surfaces were fully O-terminated prior to use, unless otherwise stated. All substrates were cleaned by sonication in acetone (≥99%; Sigma Aldrich, St Louis, USA) (except for PVC and SPC), followed by isopropanol (≥99.5%; Sigma Aldrich, St Louis, USA) (except for SPC), and Milli-Q ultrapure water (Merck Millipore, Watford, UK). All cleaning steps had a duration of 10 min. Substrates were wiped with lint-free cloth between solvents and stored in 70% ethanol until further use.

Diamond substrate modification. Diamond and BDD substrates were H-terminated in a Seki Diamond 6500 series microwave plasma chemical vapor deposition system (Cornes Technologies, San Jose, USA). The substrates were evacuated to a base pressure of >1×10^{-6} mbar. Plasma hydrogenation was carried out at 500 sccm hydrogen flow, 1500 W microwave power, and 50 Torr pressure. Diamond and BDD substrates were surface roughened using a

laser micromachining approach (E-355H-3-ATHI-O, Oxford Lasers, Didcot, UK). Briefly, the laser was rastered over the surface of the substrates using a pulse density of 2×10^6 cm^{-2} and a fluence of 14 J cm^{-2}. Substrates were subsequently subjected to the acid cleaning procedure described above and then thermally oxidized in air at 600 °C for 5 h to remove any surface sp^2 carbon introduced from the laser micromachining process.

Substrate characterization. Contact angle values were measured by the static sessile drop method, using a KRÜSS DSA100 drop shape analysis system (KRÜSS GmbH, Hamburg, Germany) at 20 °C with 3 µL droplets (contact area 1-3 mm) of Milli-Q ultrapure water (Merck Millipore, Watford, UK). Surface roughness measurements were made using atomic force microscopy (AFM; Bruker Innova, Coventry, UK) operating in tapping mode using an antimony doped silicon probe with a spring constant of 3 N m^{-1}. Images were obtained at a line scan rate of 0.3 Hz with a resolution of 512 lines and 512 points per line. For each substrate, three 5×5 µm areas were scanned (n = 3) and images analyzed using Scanning Probe Image Processor (SPIP) software (v. 6.0.14, Image Metrology, Hørsholm, Denmark).

Bacterial strains, media and growth conditions. Ten waterborne or water-based biofilm-producing bacterial strains were included in this study: *P. aeruginosa* MPAO1, *P. aeruginosa* NPAO1, *P. aeruginosa* PA14, *P. aeruginosa* LESB58, *P. aeruginosa* ΔwspF (hyperaggregative phenotype), *P. aeruginosa* ΔPsl ΔPel (non-biofilm producer phenotype), *Acinetobacter baumannii* DSM 30008, *Aeromonas hydrophila* DSM 30187, *Klebsiella pneumoniae* DSM 30104, and *Staphylococcus aureus* ATCC 29213. All of these strains have been widely used for biofilm studies, are known to be moderate to strong biofilm producers, and are well characterized for genotype and phenotype.[44–47] All strains were stored as frozen stocks (−80 °C freezer) in Luria-Bertani (LB) broth (containing 10 g L^{-1} sodium chloride) with 20% glycerol until future use.

Inocula preparation and biofilm formation. Substrates were removed from 70% ethanol immersion and placed individually into the bottom of the wells of a polystyrene microtiter plate (Corning, Durham, USA). Three discs of each substrate were used per strain, in order to obtain triplicate measurements ($n = 3$). To confirm assay sterility, *i.e.* substrates are completely sterile, 200 µL of LB medium were added to each well and the microtiter plate incubated under static conditions at 37 °C for 24 h. Bacterial strains were transferred from the stock cultures to LB agar plates and incubated aerobically at 37 °C for 18 to 24 h. All strains were subcultured to LB broth and incubated at 37 °C, 120 rpm. The optical density of the bacterial cultures was monitored at 600 nm (OD_{600}) using a Jenway 7200 spectrophotometer (Cole-Parmer, Staffordshire, UK) to ensure that all cultures reached a mid-exponential growth phase, with an OD_{600} corresponding to approximately 10^8 cells mL^{-1} (strain-dependent OD_{600} range: 0.15–0.2). The strain *P. aeruginosa* ΔPsl ΔPel was used solely for validation of the microtiter plate biofilm assay, as this strain should not produce biofilm and therefore acts as a negative control. All other *Pseudomonas* strains were studied as monospecies biofilm producers. *P. aeruginosa* MPAO1 and the four non-*Pseudomonas* strains were used to generate multispecies biofilms.

Bacterial strains were tested for their ability to form biofilm on the substrates in the presence of two different media: LB broth (pH = 6.9 ± 0.1) and filtered tap drinking water (pH = 6.8 ± 0.1). The tap drinking water was collected from University of Warwick, Coventry, UK and filtered using a 0.2 µm pore-size membrane filter (Sartorius Stedim Biotech, Göttingen, Germany). Free chlorine test strips (Fisher Scientific, Loughborough, UK) showed no free chlorine present in the drinking water (<0.05 ppm limit of detection). For the assay with LB growth medium, a 200 µL bacterial inoculum was added to each well (2×10^7 cells $well^{-1}$) after aspiration of LB previously added for sterility testing. For the assay with drinking water as the growth medium, the inoculum was centrifuged at 7,500 rpm for 10 min, the supernatant was

removed and the bacterial pellet resuspended in the filtered tap water. The inoculum with a volume of 200 µL was then added to each well (2×10^7 cells well^{-1}).

For multispecies biofilms, a similar procedure was followed with equal cell concentrations of each strain being mixed together to attain the final inoculum of approximately 2×10^7 cells well^{-1}. For every assay, the microtiter plate was incubated under static conditions at either 37 °C or 20 °C for 2 days. For each substrate, negative controls (n = 3, medium only) were included. For each strain, positive growth controls (n = 3, absence of substrate) were also present in the analysis.

Microtiter plate biofilm formation quantitative assay. The assay was adapted from previously described protocols.[45,48,49] Briefly, after the 2 day-incubation, 150 µL of the liquid culture comprising planktonic cells were carefully aspirated from each well. Next, wells containing the substrate were washed once with sterile water, then the biofilm was fixed by incubation at 70 °C for 1 h. Substrates were transferred using sterile tweezers to a new 96-well plate, before being stained with 200 µL of 0.1% crystal violet aqueous solution (1% in H_2O; Sigma Aldrich, St Louis, USA) for 15 min. The stain was removed from the wells and washed three times with sterile water to remove excess. Stained biofilm was solubilized in 200 µL of 30% acetic acid (≥99.7%; Fisher Scientific, Loughborough, UK) for 15 min. The solubilized stain was transferred to a new 96-well plate and the absorbance at 595 nm (A_{595}) measured using a Multiskan FC Microplate Photometer (Fisher Scientific, Loughborough, UK).

Confocal laser scanning and scanning electron microscopy. For all microscopy analysis, only MPAO1 monospecies and multispecies biofilms were investigated as MPAO1 is the most frequently studied *P. aeruginosa* strain. Processing of the substrates for microscopy analysis comprised different fixation and staining steps. The washing step was followed by chemical fixation with 200 µL of 1% glutaraldehyde (Grade I, 50% in H_2O; Sigma Aldrich, St Louis, USA) for 1 h. To remove excess glutaraldehyde, a three-step washing with 200 µL of sterile

water was additionally performed. These sample pre-treatment steps were common to both microscopy techniques.

For CLSM, biofilm cells were stained by the addition of 150 µL of 0.1 mg mL^{-1} propidium iodide (≥94%; Sigma Aldrich, St Louis, USA) for 15 min at room temperature. A washing step with sterile water followed. Substrates were transferred using sterile tweezers onto a microscope slide. The dead stained biofilm cells were visualized on a Zeiss LSM710 microscope (Carl Zeiss Ltd., Cambridge, UK). A diode-pumped solid-state laser with maximum emission at 561 nm was used as the excitation source, whilst the detection range was 566–718 nm. Triplicate images were obtained across two independent samples. Images were analyzed using ImageJ software (v. 1.51n, National Institutes of Health, USA) by individually thresholding each image slice of the *z* stack, summing the slices, and calculating the mean fluorescence intensity across the resultant image.

For SEM, biofilms were dehydrated by a graded series of ethanol (50, 75, 90, 95, and 100%) for 10 min each. PVC substrates were carbon coated prior to imaging (Emitech K950X sputter coater, Quorum Technologies, Kent, UK). Images were obtained using the secondary electron detector on a Zeiss Gemini field emission (FE) instrument (Carl Zeiss Ltd., Cambridge, UK) operating at 1 kV. A minimum of 10 images were obtained per sample.

Statistical analysis. Statistical analysis was performed using Past3 (v. 3.16, Oslo, Norway). To evaluate statistical correlations and identify trends in biofilm formation across substrates, Spearman's rank correlation (r_s) test was performed. To evaluate statistical differences in biofilm formation between substrates, either the paired *t* test was performed (for comparisons between two sets of observations), or the Kruskal-Wallis test with Dunn's post hoc adjusted for Bonferroni correction (for comparisons across all substrates). Data sets underwent the Shapiro-Wilk test for normal distribution prior to the aforementioned statistical tests. Differences were considered statistically significant at a probability $p < 0.05$.

RESULTS and DISCUSSION

***P. aeruginosa* monospecies biofilm formation on substrates.** The ability of *five* different *P. aeruginosa* strains to form biofilms on the substrates under study was assessed. All measurements were carried out at one fixed growth time (48 h), thereby focusing predominantly on initial bacterial adhesion and the early stages of biofilm development. After incubation, similar growth of free-floating bacteria in the medium (planktonic bacterial growth) was overall observed in the presence of all substrates, with the exception of copper where a comparatively lower planktonic bacterial growth was mostly detected (data not shown).

To quantify the extent of biofilm formation on each substrate, a microtiter CV assay was used, whereby the absorbance of the solubilized CV stain (A_{595}) is considered proportional to the amount of biofilm biomass on the surface. CV absorbance data for these monospecies biofilms are summarized in box plot form in **Figure 1**, and the individual CV absorbance data of each strain used is detailed in **Figure S1, SI1**. The absorbance data has been normalized with respect to geometric surface area. All substrates, except for SPC, had the same geometric surface area. The approach was employed in two different growth media, nutrient rich LB medium (high ionic strength) and low-nutrient drinking water (low ionic strength) to mimic environmental conditions, under two different temperature conditions, 37 °C (optimum bacterial growth temperature) and 20 °C (closer to environmental water temperature).

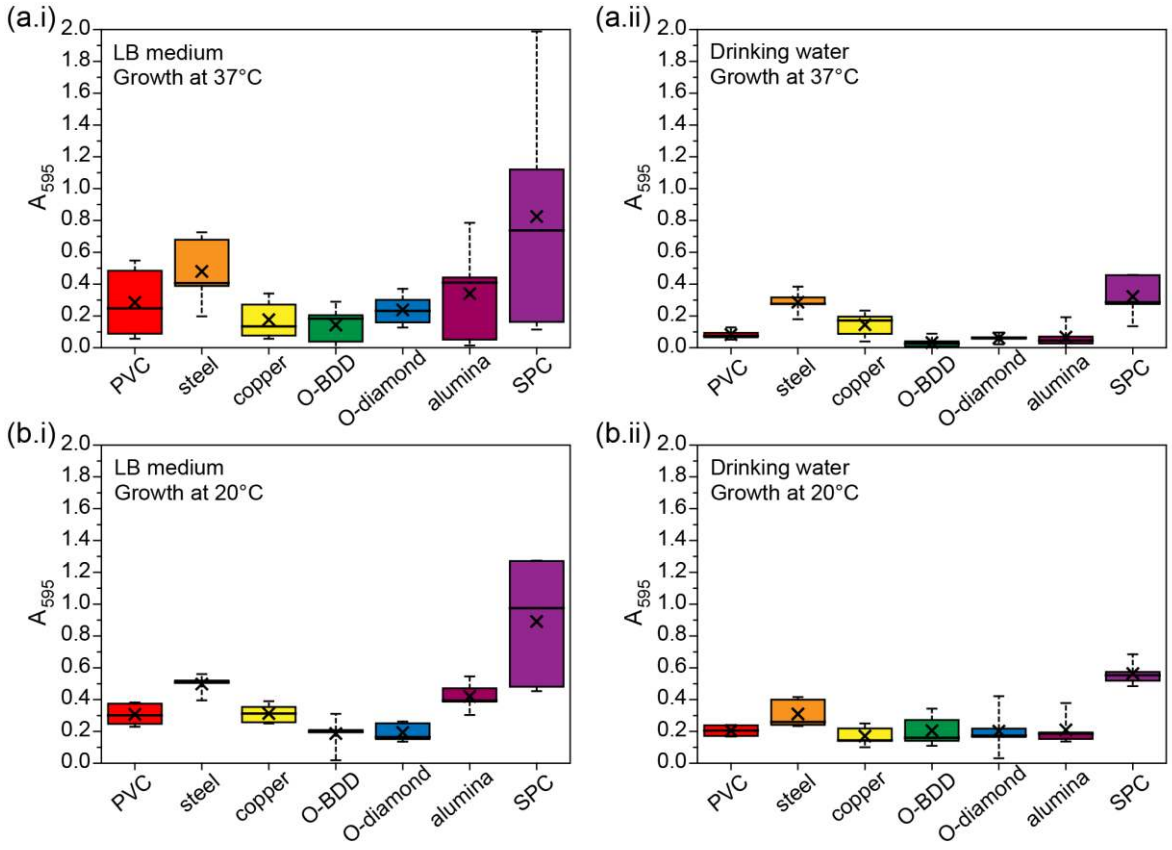

Figure 1. Extent of *P. aeruginosa* monospecies biofilm formation on different substrates. Data expressed as the absorbance of solubilized CV stain at 595 nm. Biofilm formation was assessed after 48 h under the following growth conditions: (a) 37 °C and (b) 20 °C, in (i) LB medium and (ii) drinking water. Data from five individual strains (MPAO1, NPAO1, PA14, LESB58, ΔwspF) is presented as a boxplot where crosses and bars indicate mean and median absorbance values respectively (n = 3 for each strain), and whiskers extend to minimum and maximum data points.

Comparison of the extent of *P. aeruginosa* monospecies biofilm formation at both 37 °C and 20 °C revealed no significant differences in the quantity of biofilm formed on each substrate in LB medium (paired t test, $p = 0.1$). A rank-order analysis of biofilm formation across all substrates showed a strong correlation ($r_s = 0.89$, $p < 0.05$), indicating a similar trend in biofilm formation across substrates independent of temperature. In drinking water, significantly higher biofilm biomass was observed at 20 °C compared to 37 °C (paired t test, $p < 0.05$) for each

substrate. Since biofilm formation is often a response to unfavorable environmental conditions or stresses,[11,50] it appears that the restricted nutrient content of drinking water in combination with a sub-optimal growth temperature has actively promoted biofilm formation under these more hostile conditions. Also, the same trend in biofilm formation across substrates at 37 °C and 20 °C was not observed (r_s = 0.46, p = 0.3). This is mostly explained by a comparatively higher biofilm formation on the copper substrate at 37 °C, where a similar planktonic bacterial growth was observed in the presence of all substrates (measured by OD_{600}).

When comparing if nutrient content could have an impact on the results obtained, we observed that the amount of biofilm formed on substrates in drinking water was significantly lower than in LB medium, regardless of temperature (paired t test, $p < 0.05$). This data confirms that for *P. aeruginosa* biofilm formation, nutrient content is important.[11,50] Comparing data for biofilm formation across all substrates, the trends between the substrates in the two different growth media were more similar at 37 °C (r_s = 0.75, p = 0.07) than at 20 °C (r_s = 0.67, p = 0.07). The substrate that showed the biggest difference in biofilm formation was alumina, showing a comparatively higher biofilm formation on its surface in LB medium than in drinking water (for both growth temperatures).

Examining individual substrates, the amount of biofilm formed on SPC was the highest in all conditions tested, reported as a mean A_{595} throughout, (= 0.65 ± 0.26). Conversely, the lowest amount of biofilm formed was observed on O-BDD (A_{595} = 0.14 ± 0.08). Between these extremes, steel was the substrate on which the second highest amount of biofilm was quantified (A_{595} = 0.39 ± 0.11), followed by alumina (A_{595} = 0.26 ± 0.15), PVC (A_{595} = 0.22 ± 0.10), copper (A_{595} = 0.20 ± 0.08), and O-diamond (A_{595} = 0.17 ± 0.08). Statistical analysis also highlighted significant differences across the substrates studied (Kruskal-Wallis, $p < 0.05$), with significantly lower biofilm formation on (1) both O-BDD and O-diamond compared to SPC and steel in LB medium at 20 °C and 37 °C; (2) O-BDD compared to SPC and steel in

drinking water at 37 °C, and (3) copper against SPC in drinking water at 20 °C (post-hoc Dunn's test, $p < 0.05$). Regarding individual *P. aeruginosa* strain biofilm formation, the measured range was substrate-specific and showed intra-species variability, with the highest overall variation in biofilm formation among strains being observed on SPC. Nonetheless, in three out of the four growth conditions employed, the highest amount of biofilm across all five strains was observed on SPC (**Figure S1, SI1**).

In addition to the quantitative CV analysis, FE-SEM was used as a complementary technique to image the biofilms formed on the substrates (**Figure 2**). FE-SEM investigation of the *P. aeruginosa* monospecies biofilms formed on all the substrates at 37 °C in LB medium qualitatively corroborated the findings of the CV assay, *i.e.* the lowest levels of biofilm formation were observed on O-BDD. On SPC a dense, uniform coating of biofilm over the entire substrate results, while for alumina the majority of the substrate is coated. On the other hand, whilst formation of biofilm on copper and steel is prevalent, it is heterogeneously distributed across the surface. When using drinking water as the growth medium (**Figure S2, SI2**), biofilm formation on all substrates was visibly lower than in LB medium, in agreement with the CV data. The most visually noticeable difference was observed with alumina (compare **Figure 2f** with **Figure S2f, SI2**), corroborating the observations from the CV assay. On PVC and both O-BDD and O-diamond substrates, in both LB medium (**Figure 2**) and drinking water (**Figure S2, SI2**), biofilm formation is sparse with only individual bacteria, with typical dimensions of *ca.* 1 μm length, visible. Whilst biofilm formation on PVC appeared heterogeneous in distribution (**Figure 3, SI3**), interestingly on both O-diamond and O-BDD, no preferential growth behavior was observed across the two surfaces, which are polycrystalline in nature.

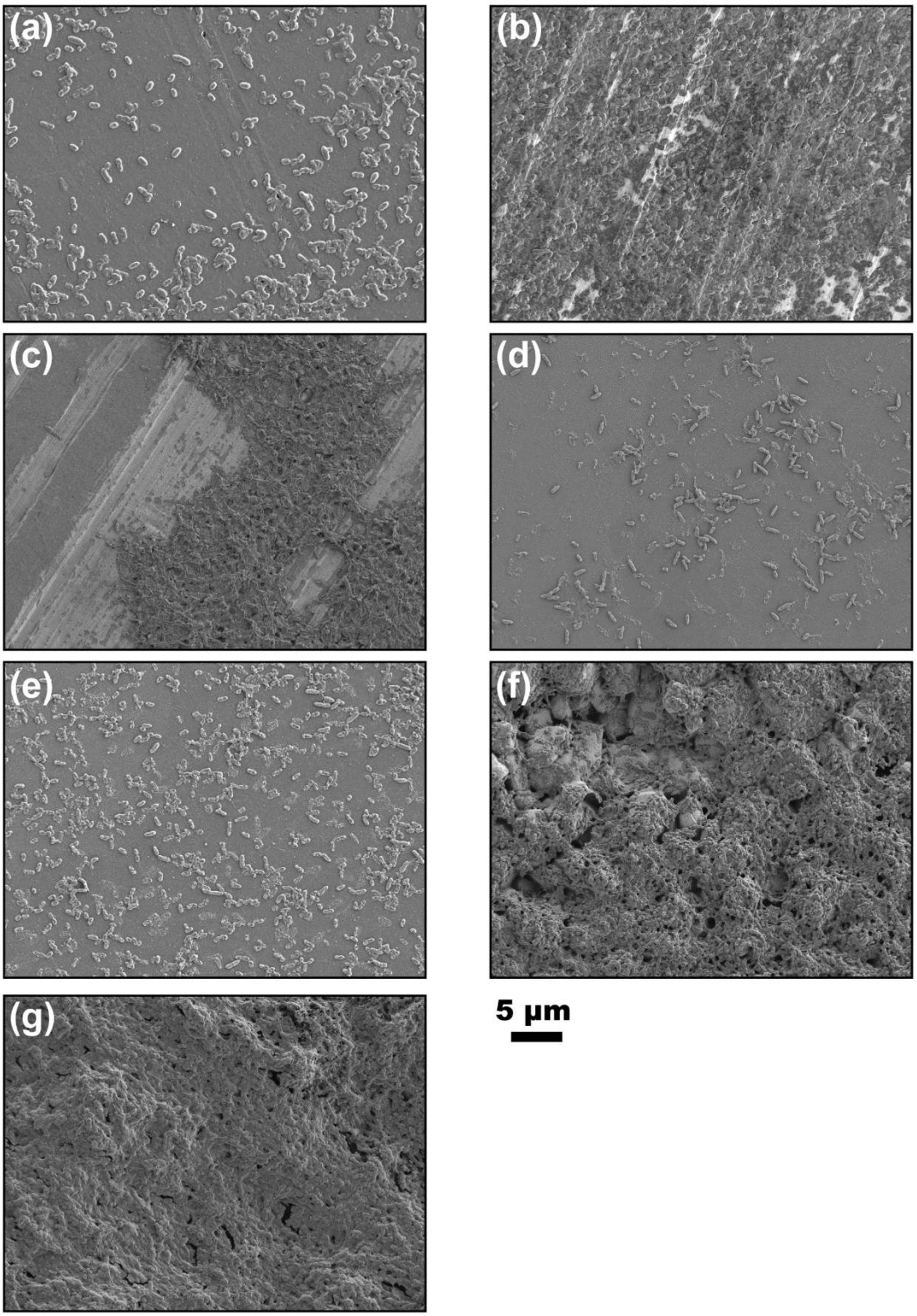

Figure 2. FE-SEM images of *P. aeruginosa* MPAO1 monospecies biofilms formed on (a) PVC, (b) steel, (c) copper, (d) O-BDD, (e) O-diamond, (f) alumina, and (g) SPC after 48 h bacterial growth in LB medium.

Surface roughness is often considered an important factor in biofilm formation, though the extent to which this property influences the process is dependent on the material, type of roughness, environmental conditions and bacterial species.[33,35–38] Substrate surface roughness (arithmetical mean roughness, R_a) was determined by AFM image analysis (**Figure S4a, SI4**). O-BDD (and O-diamond) substrates presented the smoothest surfaces, having a sub-nanometer level roughness, whilst alumina and SPC were more than two orders of magnitude rougher (Table 1). FE-SEM images of the bare surfaces are presented in **Figure S4b, SI4**.

Table 1. Surface roughness measurements of the substrates used.

Substrate	Surface roughness, R_a / nm
PVC	4.76 ± 0.78
Steel	23.7 ± 3.0
Copper	23.0 ± 5.0
O-BDD	0.49 ± 0.04
O-Diamond	0.72 ± 0.16
Alumina	208 ± 50
SPC	204 ± 35

Values listed as mean ± SD (n = 3).

The extent of *P. aeruginosa* monospecies biofilm formation was highest on SPC, which has the highest surface roughness (comparable with alumina), most likely due to the increased number of attachment sites.[33,36,37,51,52] In contrast, the lowest biofilm formation observed, under almost all conditions, was with O-BDD which exhibited the lowest surface roughness. In this case the smooth surfaces are likely to be presenting lower obstacle densities, enabling the bacteria to spread more[53,54] and making it more difficult for the bacteria to find each other to begin building a community (biofilm),[11,55–57] as observed in the FE-SEM images (**Figures 2d** and **e**).

To better account for surface roughness, the CV absorbance data was normalized against total surface area, as determined from the AFM image analysis (**Table S1, SI4**), and shown in **Figure S5, SI5**. Even after total surface area normalization, similar trends are still revealed. SPC (A_{595} = 0.037 ± 0.015 mm^{-2}) consistently shows the highest amount of biofilm, whilst O-BDD showed the lowest amount of biofilm (A_{595} = 0.011 ± 0.006 mm^{-2}). Thus, surface roughness alone cannot be responsible for the differences observed as even when correcting for total surface area, O-BDD outperforms SPC in terms of minimizing biofilm formation on the surface.

Multispecies biofilm formation on substrates. In order to ensure a greater ecological relevance, the extent of multispecies biofilm formation on the seven substrates was investigated. Four different bacterial species (*A. baumannii*, *A. hydrophila*, *K. pneumoniae* and *S. aureus*) along with *P. aeruginosa* MPAO1 were co-cultured. Incubation in the presence of all substrates under study was conducted at 37 °C in both LB medium and drinking water. The microtiter assay absorbance values of the solubilized CV of destained biofilms were determined as a quantitative measurement (five technical replicates) of the multispecies biofilm formed (**Figure 3**). Accordingly, the absorbance values represent total biofilm biomass formed and no information can be extracted regarding the species dependence (the proportion of each bacterial species that make up the total multispecies biofilm) of each substrate.

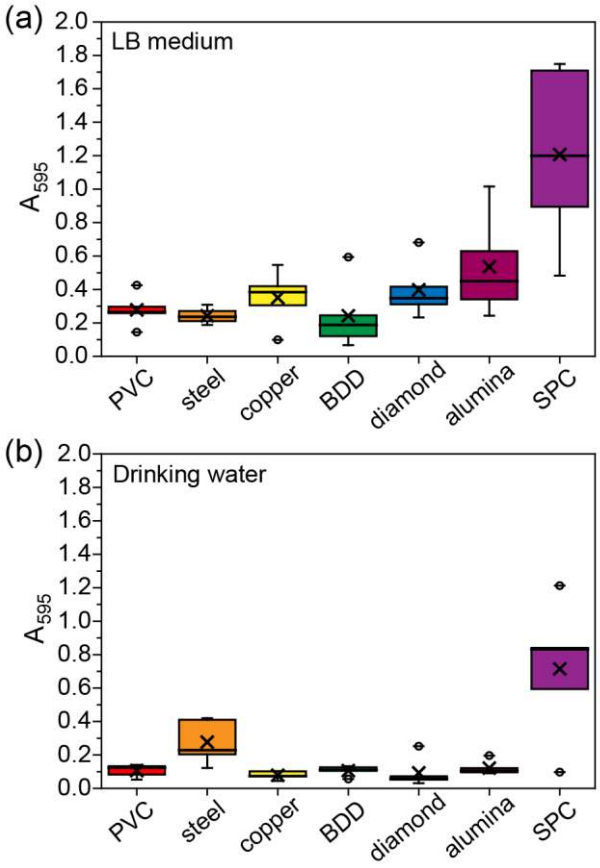

Figure 3. Extent of multispecies biofilm formation on different substrates. Data expressed as the absorbance of solubilized CV stain at 595 nm. Biofilm formation was assessed after 48 h at 37 °C in (a) LB medium and (b) drinking water. Data from five replicates is presented as a boxplot, where crosses and bars indicate mean and median absorbance values respectively, whiskers extend to values within 1.5 times the interquartile range, and circles specify outliers.

Comparison of the overall amount of multispecies biofilm formed with the overall amount of *P. aeruginosa* MPAO1 monospecies biofilm revealed that there was no significant difference in the quantity (biomass) of biofilm formed in either LB medium or drinking water (paired *t* test, $p = 0.2$ and 0.1, respectively). These findings suggest that interspecific interactions of cooperative or competitive nature between bacterial species did not substantially impact biofilm formation over the duration of the experiment.[58,59] Similar to the *P. aeruginosa* monospecies biofilm data, the amount of multispecies biofilm formed in the presence of drinking water was significantly lower than in LB medium (paired *t* test, $p < 0.05$). A rank-

order comparative analysis of the multispecies biofilm formation across substrates also revealed a statistical dependence on the growth media (r_s = 0.11, p = 0.78). When performing the experiments in LB, the lowest amount of multispecies biofilm was detected on O-BDD (A_{595} = 0.24 ± 0.21) while the highest biofilm biomass was detected on SPC (A_{595} = 1.21 ± 0.54), corroborating the results of *P. aeruginosa* MPAO1 monospecies biofilm (**Figure S1, SI1**). The amount of biofilm on SPC was approximately three times higher than most other substrates, but was only statistically significantly higher than BDD (Kruskal-Wallis, $p < 0.05$; post-hoc Dunn's test, $p < 0.05$). The experiments in drinking water similarly showed the highest amount of multispecies biofilm biomass on SPC (A_{595} = 0.72 ± 0.41). The substrate with the second highest multispecies biomass was steel (A_{595} = 0.28 ± 0.13), with all other substrates showing comparable values (A_{595} = 0.10 ± 0.02).

P. aeruginosa **biofilm formation on modified diamond substrates.** To understand the origins of the low biofouling characteristics of O-BDD, further studies were carried out to assess the impact of both boron doping and surface termination on biofilm formation at 37 °C in LB medium on modified BDD substrates. The surface roughness of the BDD/diamond substrates employed for these studies was kept very similar, in order to exclude roughness effects (**Table 2**). Undoped and metal-like doped BDD substrates were employed along with O- and H-terminated BDD/diamond. After chemical vapor deposition growth in the hydrogen environment, the BDD/diamond leaves the growth chamber terminated with C–H groups.[23] The O-terminated polycrystalline surface presents a variety of different oxygen functional groups including C=O, C–O–C and C–OH.[23] Experiments also explored the effect of deliberately increasing the surface roughness of O-terminated BDD/diamond, using a laser roughening approach. FE-SEM images of the bare substrates are found in **Figure S6, SI6**.

Table 2. Physical properties of the diamond and BDD substrates.

Substrate	Contact angle / °	Surface roughness, R_a / nm
O-BDD (smooth)	25.5 ± 1.7	0.49 ± 0.04
O-BDD (rough)	22.6 ± 4.9	118 ± 11
H-BDD (smooth)	117.5 ± 6.5	0.18 ± 0.01
O-Diamond (smooth)	34.2 ± 0.3	0.72 ± 0.16
O-Diamond (rough)	26.7 ± 7.0	100 ± 30
H-Diamond (smooth)	96.3 ± 5.3	0.63 ± 0.21

Contact angle and surface roughness values listed as mean ± SD (n = 3).

Water contact angle measurements, which represent the interplay between polar and dispersion substrate-water interactions,[60] were recorded on all the BDD and diamond substrates to provide information on the hydrophobicity/hydrophilicity of the surface (**Table 2**). Interestingly, O-BDD shows the lowest contact angle of all surfaces examined, including those of the other materials investigated (**Table S1, SI3**), indicating that it is the most hydrophilic. In contrast, the H-BDD surface presents the most hydrophobic surface, demonstrating the huge changes in wettability possible on a BDD/diamond surface simply by changing the surface termination. Importantly, this can take place under conditions which leave the substrate topography[23] and mechanical properties (stiffness)[36] unchanged.

To determine the quantity of biofilm formed on the surface of the modified diamond and BDD substrates, CLSM was applied.[8,43] Whilst CV assays are useful, the values obtained for the destained *P. aeruginosa* monospecies and multispecies biofilm on BDD (and diamond) were close to the detection limit of the technique. Thus, to more precisely assess the impact of the surface roughness and hydrophobicity on biofilm formation, quantitative analysis of the fluorescence intensity from the CLSM images was undertaken for the modified diamond substrates (**Figure 4**) in addition to the original substrates (**Figure S7, SI7**). A strong positive

correlation was observed between CLSM and CV assay results for both *P. aeruginosa* monospecies and multispecies biofilm formation on all substrates (r_s = 0.8, p < 0.1), largely supporting the use of either of the quantitative methods for comparative studies.

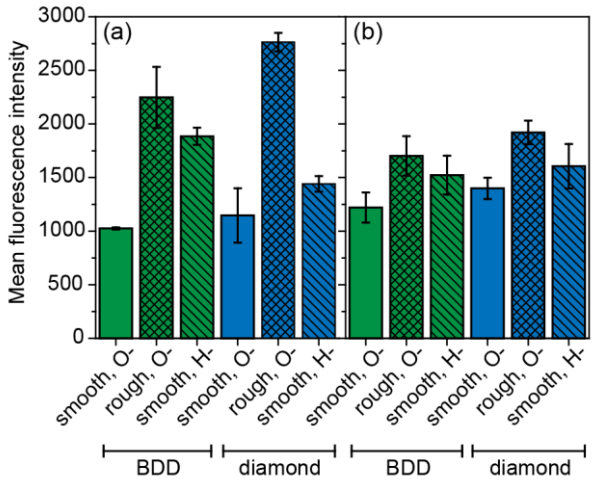

Figure 4. Fluorescence intensity of propidium iodide stained (a) *P. aeruginosa* monospecies and (b) multispecies biofilms formed on modified diamond substrates. BDD and diamond substrates were modified to have three different surface characteristics: O-terminated (hydrophilic) and smooth, O-terminated and rough, and H-terminated (hydrophobic) and smooth. Biofilm formation determined after 48 h bacterial growth at 37 °C in LB medium. CLSM images of the biofilms were obtained, and each image was analyzed to record the mean fluorescence intensity of propidium iodide at 566–718 nm. Bars represent mean ± SD (n = 3).

For O-termination, when evaluating the rough O-BDD and rough O-diamond with their smooth analogues, the extent of *P. aeruginosa* monospecies biofilm formation was significantly greater (t test, p < 0.05) on the rough compared to smooth surfaces. The mean fluorescence intensity was approximately 2.2 and 2.4 times higher, for O-BDD and O-diamond, respectively, compared to the smooth O-surfaces. Previous *P. aeruginosa* SEM studies with nanocrystalline and microcrystalline diamond (same surface termination) found the numbers of adhering bacteria were greater for microcrystalline diamond than nanodiamond (rms roughness 88.9 nm and 49.9 nm, respectively).[30] Based on our studies, we speculate that this

is most likely due to surface roughness increasing attachment sites on the surface. Although we note, there may also be changes in the chemical functionality of the surface occurring during the roughening process, which can also influence bacterial adhesion.[36,61]This could account for the slightly increased hydrophilicity of the rough O-BDD and O-diamond compared to their smooth counterparts.

When comparing the smooth H-terminated BDD and smooth H-diamond with their O-terminated smooth equivalents, the amount of biofilm formed was noticeably higher (*t* test, $p < 0.05$) on H-terminated substrates, clearly showing the role that this factor plays under conditions independent of surface roughness. The average fluorescence intensity was 1.8 times and 1.3 higher on H-terminated smooth BDD and H-diamond, respectively, compared to their O-terminated counterparts. Note that the hydrophobicity of H-BDD was greater than H-diamond (**Table 2**). The extent of multispecies biofilm formation on the modified diamond substrates was also significantly greater on the rough O-BDD and rough O-diamond substrates than on the smooth O-BDD and O-diamond surfaces (*t* test, $p < 0.05$), with the mean fluorescence intensity 1.4 times higher for both rougher substrates. The extent of multispecies biofilm formation on the H-BDD and H-diamond smooth substrates was marginally greater than the O-terminated smooth BDD and diamond surfaces (*t* test, $p = 0.08$ for BDD, $p = 0.2$ for diamond).

FE-SEM performed on all BDD and diamond substrates largely support the CLSM data, and representative images are shown in **Figure 5** for *P. aeruginosa* monospecies. Further FE-SEM imaging of multispecies biofilm formation on all the substrates used in this study are shown in **Figure S8, SI8**. As shown by **Figure 5**, biofilm formation on the rough O-BDD and rough O-diamond substrates resulted in a thicker, uniform biofilm structure. Conversely, the O-terminated smooth substrates showed adhesion of individual bacteria but little evidence of biofilm formation and colonization. Biofilms on the smooth H-BDD and H-diamond were

heterogeneous across the substrates, but have noticeably increased bacterial cell density compared to their O-smooth counterparts though are not as dense as the O-rough diamond and BDD surfaces.

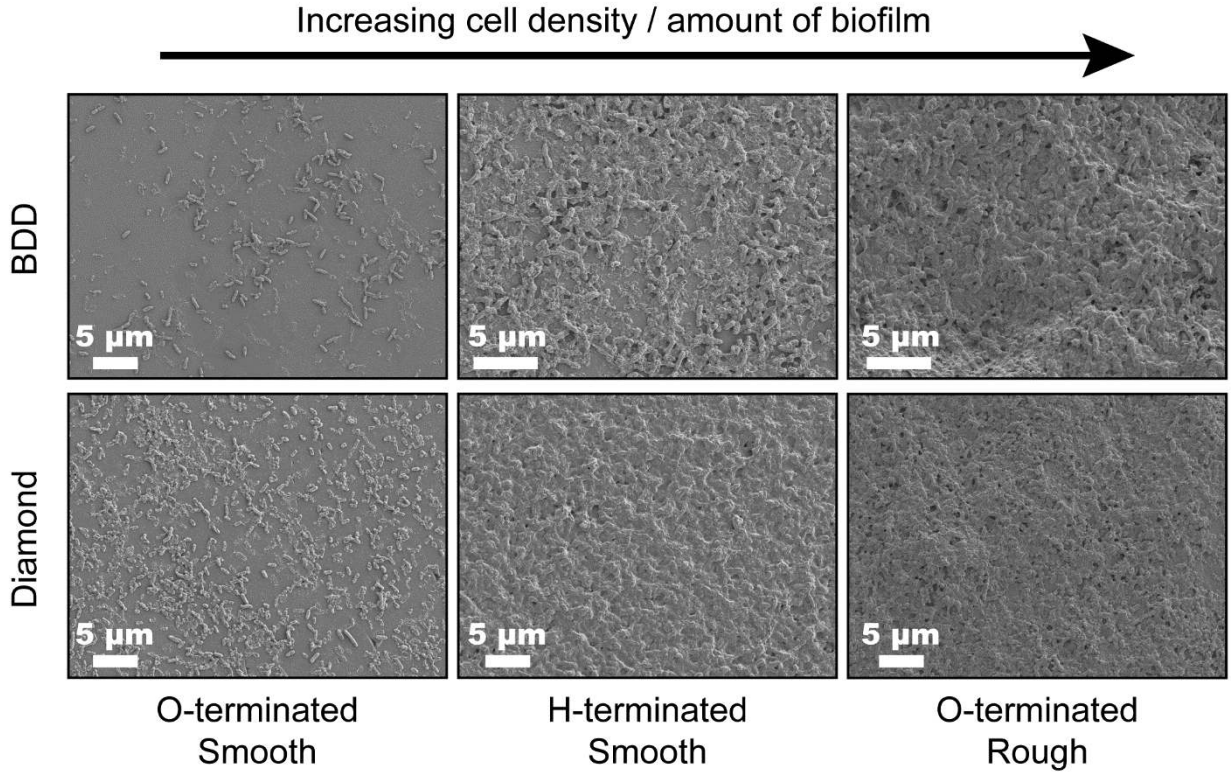

Figure 5. FE-SEM images of *P. aeruginosa* monospecies biofilms formed on BDD and diamond, with three different surface characteristics: O-terminated (hydrophilic) and smooth, H-terminated (hydrophobic) and smooth, and O-terminated and rough.

It is clear from the results presented that surface termination on BDD and diamond plays a significant role in influencing bacteria attachment and biofilm formation capabilities, with H-termination strongly favoring biofilm formation. This suggests that *P. aeruginosa* and the multispecies bacteria are presenting a more hydrophobic outer cell wall to the surface, resulting in favorable hydrophobic and non-polar interactions, along with weak van der Waals interactions.[33,34,38,56,62–64] For water on H-diamond, simulations[65] have shown that although the C–H bond on diamond is polarized ($C^{\delta-}$—$H^{\delta+}$), it only acts as a weak hydrogen bond donor

with water. It is the dispersion forces that dominate significantly over any electrostatic contribution, leading to low adsorption energies for water and a high contact angle. In contrast, for O-diamond the bond polarity is reversed ($C^{\delta+}$—$O^{\delta-}$)[23,66] and strong electrostatic hydrogen bonding effects are now significant, leading to much greater water adsorption energies and a lower contact angle. It is these extreme properties that are likely to be disfavoring adhesion of the hydrophobic bacteria to the O-terminated surface.[67] Additionally, since bacterial cell walls are mostly negatively charged,[51] we also believe that bond polarity (dipole) of the $C^{\delta+}$—$O^{\delta-}$ bond plays a role in reducing adhesion of the bacteria on O-BDD (and O-diamond). This repulsive effect is likely to be affected by the ionic strength of the growth medium.[38,51] Considering the application of BDD to electrochemical sensing in aquatic environments,[6,68] in future work we aim to investigate extensively the roles that electrostatics and surface potential have on bacterial adherence and biofilm formation on BDD, especially as a route to minimize biofouling even further.

Importantly, we also show that doping diamond with boron affects bacterial attachment. For example, comparing O-BDD with O-diamond, qualitative FE-SEM investigation (**Figure 5**) and quantitative CLSM analysis (**Figure 4**) both indicate a lower bacterial cell density on the boron doped surface, whilst the opposite is true for the H-terminated BDD surface. We find doping with BDD renders the O-terminated surface more hydrophilic (lower contact angle, **Table 2**), and the H-terminated more hydrophobic (higher contact angle, **Table 2**), highlighting again the role hydrophilicity/hydrophobicity (and associated factors) play for diamond/BDD substrates. Although we cannot be sure of the exact origin of the changes in wettability due to boron doping, there are a variety of possible influences which affect the way water interacts with the BDD surface, which in turn affects bacterial adhesion. These include the role of boron in withdrawing electron density between surface C and –O or –H bonds, as well as surface electrolyte potential and electron charge distribution (density of states) differences.[69] Future

studies will look to model the BDD-water interface to determine the exact origin of this phenomenon.

CONCLUSIONS

A comprehensive, systematic study of bacterial biofilm formation has been carried out using five different strains of *P. aeruginosa,* in order to compare monospecies biofilm formation on O-BDD with PVC, stainless steel, copper, O-diamond, alumina, and SPC as a function of growth medium (LB *vs.* drinking water) and temperature (37 °C *vs.* 20 °C). Further studies also investigated *A. baumannii*, *A. hydrophila*, *K. pneumoniae* and *S. aureus* bacterial multispecies biofilm formation. SPC was consistently found to have the highest amount of biofilm formation, whereas O-BDD was found to have the relatively lowest levels. Similar trends were observed even after correcting for total surface area, indicating surface roughness is not the only factor controlling bacterial adhesion and biofilm formation.

Analysis of surface hydrophobicity revealed that O-BDD was the most hydrophilic surface, due to strong electrostatic interactions with water, providing evidence for hydrophilicity (and associated factors) being very important in reducing biofilm growth for these bacteria on this surface. This was further confirmed by keeping surface topography fixed and switching surface termination to H-, which is strongly hydrophobic, and observing increased biofouling. Importantly, boron doping was also found to play a role with boron presence resulting in either increased or decreased hydrophilicity (compared to un-doped diamond), dependent on whether the surface was O- or H- terminated, respectively.

This study highlights the importance of O-BDD as a low biofouling electrode for long-term electrochemical monitoring in aquatic environments. Whilst the high hydrophilic properties are clearly advantageous, to fully realize O-BDD's low biofouling capabilities the surface should also be prepared as smooth as possible, conclusions that can also be extended to other materials

used as electrodes or electrode packaging, for this bacterial system. We anticipate that further reductions in the low biofouling attributes of O-BDD will be possible by exploiting biasing at an electrochemical potential during rest periods in the electrochemical sensing procedure, to prevent bacterial adhesion via electrostatic repulsion.

ASSOCIATED CONTENT

Supporting Information. Individual strain *P. aeruginosa* monospecies biofilm formation on substrates. FE-SEM images of *P. aeruginosa* monospecies biofilm formation on substrates. AFM, FE-SEM and Contact Angle Characterization of substrate surfaces. *P. aeruginosa* monospecies biofilm formation normalized by total surface area. Characterization of modified diamond substrates. Fluorescence studies of biofilm formation on substrates. FE-SEM images of multispecies biofilm formation on substrates (PDF)

AUTHOR INFORMATION

Corresponding Author

*Julie V. Macpherson (j.macpherson@warwick.ac.uk)

Author Contributions

JVM, EMHW and RPAP designed the study and experiments. LJS performed the experiments. LJS and RPAP analyzed the data. The manuscript was written through contributions of all authors. All authors have given approval to the final version of the manuscript.

Funding Sources

LJS thanks EPSRC for a PhD studentship through the EPSRC Centre for Doctoral Training in Molecular Analytical Science, grant number EP/L015307/1, and the Defense Science and Technology Laboratory. EMHW and RPAP were in receipt of EU funding from FAPIC

634137, H2020-PHC-2014. JVM thanks the Royal Society for an Industry Fellowship (INF/R1/180026).

ACKNOWLEDGMENT

The authors acknowledge Freya Harrison (Life Sciences, Warwick) and Matthew R. Parsek (Microbiology, Washington) for providing us with the *P. aeruginosa* strains used in this study. The authors thank Mareike Herrmann (Chemistry, Warwick) for substrate preparation, Sam Cobb (Chemistry, Warwick) and Oliver Williams (Physics, Cardiff) for preparation of the modified diamond substrates, Haytham Hussein (Chemistry, Warwick) for assistance with AFM and SEM, Nicole Reily (Chemistry, Warwick) for help with CV and SEM assays, and Ian Hands-Portman (Life Sciences, Warwick) for help and advice with CLSM and image analysis.

ABBREVIATIONS

AFM, atomic force microscopy; BDD, boron doped diamond; CLSM, confocal laser scanning microscopy; CV, crystal violet; FE, field emission; LB, Luria-Bertani; PVC, polyvinyl chloride; SD, standard deviation; SEM, scanning electron microscopy; SPC, screen printed carbon.

REFERENCES

(1) *In Situ Monitoring of Aquatic Systems: Chemical Analysis and Speciation*, 1st ed.; Buffle, J., Horvai, G., Eds.; John Wiley & Sons, Inc.: Chichester, 2001.

(2) Howell, K. A.; Achterberg, E. P.; Braungardt, C. B.; Tappin, A. D.; Worsfold, P. J.; Turner, D. R. Voltammetric in Situ Measurements of Trace Metals in Coastal Waters. *TrAC - Trends Anal. Chem.* **2003**, *22* (11), 828–835. https://doi.org/10.1016/S0165-9936(03)01203-2.

(3) Prien, R. D. The Future of Chemical in Situ Sensors. *Mar. Chem.* **2007**, *107* (3), 422–

432. https://doi.org/10.1016/j.marchem.2007.01.014.

(4) Delauney, L.; Compère, C.; Lehaitre, M. Biofouling Protection for Marine Environmental Sensors. *Ocean Sci.* **2010**, *6* (2), 503–511. https://doi.org/10.5194/os-6-503-2010.

(5) Klahre, J.; Flemming, H. C. Monitoring of Biofouling in Papermill Process Waters. *Water Res.* **2000**, *34* (14), 3657–3665. https://doi.org/10.1016/S0043-1354(00)00094-4.

(6) Flemming, H. C. Microbial Biofouling: Unsolved Problems, Insufficient Approaches, and Possible Solutions. In *Biofilm Highlights*; Flemming, H. C., Wingender, J., Szewzyk, U., Eds.; Springer-Verlag: Berlin, 2011; pp 81–110.

(7) Flemming, H. C. Biofouling in Water Systems - Cases, Causes and Countermeasures. *Appl. Microbiol. Biotechnol.* **2002**, *59* (6), 629–640. https://doi.org/10.1007/s00253-002-1066-9.

(8) Lewandowski, Z.; Beyenal, H. *Fundamentals of Biofilm Research*, 2nd Ed.; CRC Press: Boca Raton, 2017.

(9) Donlan, R. M. Biofilm Formation: A Clinically Relevant Microbiological Process. *Clin. Infect. Dis.* **2001**, *33* (8), 1387–1392. https://doi.org/10.1086/322972.

(10) Costerton, J. W.; Cheng, K.-J.; Greesy, G. G.; Ladd, T. I.; Nickel, J. C.; Dasgupta, M.; Marrie, T. J. Bacterial Biofilms in Nature and Disease. *Ann. Rev. Microbiol.* **1987**, *41*, 435–464. https://doi.org/10.1146/annurev.mi.41.100187.002251.

(11) O'Toole, G.; Kaplan, H. B.; Kolter, R. Biofilm Formation as Microbial Development. *Annu. Rev. Microbiol.* **2000**, *54* (1), 49–79. https://doi.org/10.1146/annurev.micro.54.1.49.

(12) Bixler, G. D.; Bhushan, B. Biofouling: Lessons from Nature. *Philos. Trans. R. Soc. A Math. Phys. Eng. Sci.* **2012**, *370* (1967), 2381–2417. https://doi.org/10.1098/rsta.2011.0502.

(13) *Biofilms - Science and Technology*, 1st Ed.; Melo, L. F., Bott, T. R., Fletcher, M., Capdeville, B., Eds.; Plenum Publishing Corporation, 1992.

(14) Carpentier, B.; Cerf, O. Biofilms and Their Consequences, with Particular Reference to Hygiene in the Food Industry. *J. Appl. Bacteriol.* **1993**, *75* (6), 499–511. https://doi.org/10.1111/j.1365-2672.1993.tb01587.x.

(15) Garrett, T. R.; Bhakoo, M.; Zhang, Z. Bacterial Adhesion and Biofilms on Surfaces. *Prog. Nat. Sci.* **2008**, *18* (9), 1049–1056. https://doi.org/10.1016/j.pnsc.2008.04.001.

(16) Wingender, J.; Flemming, H. C. Biofilms in Drinking Water and Their Role as Reservoir for Pathogens. *Int. J. Hyg. Environ. Health* **2011**, *214* (6), 417–423. https://doi.org/10.1016/j.ijheh.2011.05.009.

(17) Kostakioti, M.; Hadjifrangiskou, M.; Hultgren, S. J. Bacterial Biofilms: Development, Dispersal, and Therapeutic Strategies in the Dawn of the Postantibiotic Era. *Cold Spring Harb. Perspect. Med.* **2013**, *3* (4), a010306–a010306. https://doi.org/10.1101/cshperspect.a010306.

(18) Chen, M.; Yu, Q.; Sun, H. Novel Strategies for the Prevention and Treatment of Biofilm Related Infections. *Int. J. Mol. Sci.* **2013**, *14* (9), 18488–18501. https://doi.org/10.3390/ijms140918488.

(19) Banerjee, I.; Pangule, R. C.; Kane, R. S. Antifouling Coatings: Recent Developments in the Design of Surfaces That Prevent Fouling by Proteins, Bacteria, and Marine Organisms. *Adv. Mater.* **2011**, *23* (6), 690–718.

https://doi.org/10.1002/adma.201001215.

(20) Gu, H.; Ren, D. Materials and Surface Engineering to Control Bacterial Adhesion and Biofilm Formation: A Review of Recent Advances. *Front. Chem. Sci. Eng.* **2014**, *8* (1), 20–33. https://doi.org/10.1007/s11705-014-1412-3.

(21) Tripathy, A.; Sen, P.; Su, B.; Briscoe, W. H. Natural and Bioinspired Nanostructured Bactericidal Surfaces. *Adv. Colloid Interface Sci.* **2017**, *248*, 85–104. https://doi.org/10.1016/j.cis.2017.07.030.

(22) Chamsaz, E. A.; Mankoci, S.; Barton, H. A.; Joy, A. Nontoxic Cationic Coumarin Polyester Coatings Prevent Pseudomonas Aeruginosa Biofilm Formation. *ACS Appl. Mater. Interfaces* **2017**, *9* (8), 6704–6711. https://doi.org/10.1021/acsami.6b12610.

(23) Macpherson, J. V. A Practical Guide to Using Boron Doped Diamond in Electrochemical Research. *Phys. Chem. Chem. Phys.* **2015**, *17* (5), 2935–2949. https://doi.org/10.1039/C4CP04022H.

(24) Joseph, M. B.; Bitziou, E.; Read, T. L.; Meng, L.; Palmer, N. L.; Mollart, T. P.; Newton, M. E.; MacPherson, J. V. Fabrication Route for the Production of Coplanar, Diamond Insulated, Boron Doped Diamond Macro- and Microelectrodes of Any Geometry. *Anal. Chem.* **2014**, *86* (11), 5238–5244. https://doi.org/10.1021/ac501092y.

(25) Ayres, Z. J.; Borrill, A. J.; Newland, J. C.; Newton, M. E.; Macpherson, J. V. Controlled sp2 Functionalization of Boron Doped Diamond as a Route for the Fabrication of Robust and Nernstian pH Electrodes. *Anal. Chem.* **2016**, *88* (1), 974–980. https://doi.org/10.1021/acs.analchem.5b03732.

(26) Meijs, S.; Alcaide, M.; Sørensen, C.; McDonald, M.; Sørensen, S.; Rechendorff, K.; Gerhardt, A.; Nesladek, M.; Rijkhoff, N. J. M.; Pennisi, C. P. Biofouling Resistance of

Boron-Doped Diamond Neural Stimulation Electrodes Is Superior to Titanium Nitride Electrodes in Vivo. *J. Neural Eng.* **2016**, *13* (5), 56011. https://doi.org/10.1088/1741-2560/13/5/056011.

(27) Wilson, R. E.; Stoianov, I.; O'Hare, D. Biofouling and in Situ Electrochemical Cleaning of a Boron-Doped Diamond Free Chlorine Sensor. *Electrochem. commun.* **2016**, *71*, 79–83. https://doi.org/10.1016/j.elecom.2016.08.015.

(28) Chong, K. F.; Loh, K. P.; Vedula, S. R. K.; Lim, C. T.; Sternschulte, H.; Steinmüller, D.; Sheu, F. S.; Zhong, Y. L. Cell Adhesion Properties on-Photochemically Functionalized Diamond. *Langmuir* **2007**, *23* (10), 5615–5621. https://doi.org/10.1021/la070037y.

(29) Kloss, F. R.; Gassner, R.; Preiner, J.; Ebner, A.; Larsson, K.; Hächl, O.; Tuli, T.; Rasse, M.; Moser, D.; Laimer, K.; Nickel, E. A.; Laschober, G.; Brunauer, R.; Klima, G.; Hinterdorfer, P.; Steinmüller-Nethl, D.; Lepperdinger, G. The Role of Oxygen Termination of Nanocrystalline Diamond on Immobilisation of BMP-2 and Subsequent Bone Formation. *Biomaterials* **2008**, *29* (16), 2433–2442. https://doi.org/10.1016/j.biomaterials.2008.01.036.

(30) Medina, O.; Nocua, J.; Mendoza, F.; Gómez-Moreno, R.; Ávalos, J.; Rodríguez, C.; Morell, G. Bactericide and Bacterial Anti-Adhesive Properties of the Nanocrystalline Diamond Surface. *Diam. Relat. Mater.* **2012**, *22*, 77–81. https://doi.org/10.1016/j.diamond.2011.12.022.

(31) Budil, J.; Matyska Lišková, P.; Artemenko, A.; Ukraintsev, E.; Gordeev, I.; Beranová, J.; Konopásek, I.; Kromka, A. Anti-Adhesive Properties of Nanocrystalline Diamond Films against *Escherichia Coli* Bacterium: Influence of Surface Termination and

Cultivation Medium. *Diam. Relat. Mater.* **2018**, *83*, 87–93. https://doi.org/10.1016/j.diamond.2018.02.001.

(32) Jakubowski, W.; Bartosz, G.; Niedzielski, P.; Szymanski, W.; Walkowiak, B. Nanocrystalline Diamond Surface Is Resistant to Bacterial Colonization. *Diam. Relat. Mater.* **2004**, *13* (10), 1761–1763. https://doi.org/10.1016/j.diamond.2004.03.003.

(33) Merritt, K.; An, Y. H. Factors Influencing Bacterial Adhesion. In *Handbook of Bacterial Adhesion: Principles, Methods, and Applications*; An, Y. H., Friedman, R. J., Eds.; Humana Press: Totowa, 2000; pp 53–72.

(34) Cerca, N.; Pier, G. B.; Vilanova, M.; Oliveira, R.; Azeredo, J. Quantitative Analysis of Adhesion and Biofilm Formation on Hydrophilic and Hydrophobic Surfaces of Clinical Isolates of *Staphylococcus Epidermidis*. *Res. Microbiol.* **2005**, *156* (4), 506–514. https://doi.org/10.1016/j.resmic.2005.01.007.

(35) Hsu, L. C.; Fang, J.; Borca-Tasciuc, D. A.; Worobo, R. W.; Moraru, C. I. Effect of Micro- and Nanoscale Topography on the Adhesion of Bacterial Cells to Solid Surfaces. *Appl. Environ. Microbiol.* **2013**, *79* (8), 2703–2712. https://doi.org/10.1128/AEM.03436-12.

(36) Song, F.; Koo, H.; Ren, D. Effects of Material Properties on Bacterial Adhesion and Biofilm Formation. *J. Dent. Res.* **2015**, *94* (8), 1027–1034. https://doi.org/10.1177/0022034515587690.

(37) Donlan, R. M. Biofilms: Microbial Life on Surfaces. *Emerg. Infect. Dis.* **2002**, *8* (9), 881–890. https://doi.org/10.3201/eid0809.020063.

(38) Tuson, H. H.; Weibel, D. B. Bacteria-Surface Interactions. *Soft Matter* **2013**, *9* (17), 4368–4380. https://doi.org/10.1039/c3sm27705d.

(39) Røder, H. L.; Sørensen, S. J.; Burmølle, M. Studying Bacterial Multispecies Biofilms: Where to Start? *Trends Microbiol.* **2016**, *24* (6), 503–513. https://doi.org/10.1016/j.tim.2016.02.019.

(40) Emmerson, A. M. Emerging Waterborne Infections in Health-Care Settings. *Emerg. Infect. Dis.* **2001**, *7* (2), 272–276. https://doi.org/10.3201/eid0702.010225.

(41) Liu, S.; Gunawan, C.; Barraud, N.; Rice, S. A.; Harry, E. J.; Amal, R. Understanding, Monitoring, and Controlling Biofilm Growth in Drinking Water Distribution Systems. *Environ. Sci. Technol.* **2016**, *50* (17), 8954–8976. https://doi.org/10.1021/acs.est.6b00835.

(42) Szewzyk, U.; Szewzyk, R.; Manz, W.; Schleifer, K.-H. Microbiological Safety of Drinking Water. *Annu. Rev. Microbiol.* **2000**, *54* (1), 81–127. https://doi.org/10.1146/annurev.micro.54.1.81.

(43) Azeredo, J.; Azevedo, N. F.; Briandet, R.; Cerca, N.; Coenye, T.; Costa, A. R.; Desvaux, M.; Di Bonaventura, G.; Hébraud, M.; Jaglic, Z.; Kačániová, M.; Knøchel, S.; Lourenço, A.; Mergulhão, F.; Meyer, R. L.; Nychas, G.; Simões, M.; Tresse, O.; et al. Critical Review on Biofilm Methods. *Crit. Rev. Microbiol.* **2017**, *43* (3), 313–351. https://doi.org/10.1080/1040841X.2016.1208146.

(44) Kukavica-Ibrulj, I.; Bragonzi, A.; Paroni, M.; Winstanley, C.; Sanschagrin, F.; O'Toole, G. A.; Levesque, R. C. In Vivo Growth of *Pseudomonas Aeruginosa* Strains PAO1 and PA14 and the Hypervirulent Strain LESB58 in a Rat Model of Chronic Lung Infection. *J. Bacteriol.* **2008**, *190* (8), 2804–2813. https://doi.org/10.1128/JB.01572-07.

(45) Andreozzi, E.; Barbieri, F.; Ottaviani, M. F.; Giorgi, L.; Bruscolini, F.; Manti, A.; Battistelli, M.; Sabatini, L.; Pianetti, A. Dendrimers and Polyamino-Phenolic Ligands:

Activity of New Molecules Against *Legionella Pneumophila* Biofilms. *Front. Microbiol.* **2016**, *7* (289), 1–16. https://doi.org/10.3389/fmicb.2016.00289.

(46) Rendueles, O.; Ghigo, J. M. Multi-Species Biofilms: How to Avoid Unfriendly Neighbors. *FEMS Microbiol. Rev.* **2012**, *36* (5), 972–989. https://doi.org/10.1111/j.1574-6976.2012.00328.x.

(47) Mah, T. C.; O'Toole, G. A. Mechanisms of Biofilm Resistance to Antimicrobial Agents. *Trends Microbiol.* **2001**, *9* (1), 34–39. https://doi.org/10.1016/S0966-842X(00)01913-2.

(48) Merritt, J. H.; Kadouri, D. E.; O'Toole, G. A. Growing and Analyzing Static Biofilms. *Curr. Protoc. Microbiol.* **2005**, *0* (1), 1B.1.1-1B.1.17. https://doi.org/10.1002/9780471729259.mc01b01s00.

(49) Chandra, J.; Mukherjee, P. K.; Ghannoum, M. A. In Vitro Growth and Analysis of Candida Biofilms. *Nat. Protoc.* **2008**, *3* (12), 1909–1924. https://doi.org/10.1038/nprot.2008.192.

(50) O'Toole, G. A. Jekyll or Hide? *Nature* **2004**, *432* (7018), 680–681. https://doi.org/10.1038/432680a.

(51) Renner, L. D.; Weibel, D. B. Physiochemical Regulation of Biofilm Formation. *MRS Bull* **2011**, *36* (5), 347–355. https://doi.org/10.1557/mrs.2011.65.Physicochemical.

(52) Awad, T. S.; Asker, D.; Hatton, B. D. Food-Safe Modification of Stainless Steel Food-Processing Surfaces to Reduce Bacterial Biofilms. *ACS Appl. Mater. Interfaces* **2018**, *10* (27), 22902–22912. https://doi.org/10.1021/acsami.8b03788.

(53) Volpe, G. G.; Volpe, G. G. The Topography of the Environment Alters the Optimal

Search Strategy for Active Particles. *Proc. Natl. Acad. Sci.* **2017**, *114* (43), 11350–11355. https://doi.org/10.1073/pnas.1711371114.

(54) Bechinger, C.; Di Leonardo, R.; Löwen, H.; Reichhardt, C.; Volpe, G. G.; Volpe, G. G. Active Particles in Complex and Crowded Environments. *Rev. Mod. Phys.* **2016**, *88* (4), 45006. https://doi.org/10.1103/RevModPhys.88.045006.

(55) Watnick, P.; Kolter, R. Biofilm, City of Microbes. *J. Bacteriol.* **2000**, *182* (10), 2675–2679. https://doi.org/10.1128/JB.182.10.2675-2679.2000.

(56) Dunne, W. M. Bacterial Adhesion: Seen Any Good Biofilms Lately? *Clin. Microbiol. Rev.* **2002**, *15* (2), 155–166. https://doi.org/10.1128/CMR.15.2.155–166.2002.

(57) MacEachran, D. P.; O'Toole, G. A. Do Not Fear Commitment: The Initial Transition to a Surface Lifestyle by Pseudomonads. In *The Biofilm Mode of Life: Mechanisms and Adaptations*; Kjelleberg, S., Givskov, M., Eds.; Horizon Bioscience, 2007; pp 23–35.

(58) Burmølle, M.; Ren, D.; Bjarnsholt, T.; Sørensen, S. J. Interactions in Multispecies Biofilms: Do They Actually Matter? *Trends Microbiol.* **2014**, *22* (2), 84–91. https://doi.org/10.1016/j.tim.2013.12.004.

(59) Lee, K. W. K.; Periasamy, S.; Mukherjee, M.; Xie, C.; Kjelleberg, S.; Rice, S. A. Biofilm Development and Enhanced Stress Resistance of a Model, Mixed-Species Community Biofilm. *ISME J.* **2014**, *8* (4), 894–907. https://doi.org/10.1038/ismej.2013.194.

(60) Bos, R.; Mei, H. C. Van Der; Busscher, H. J. Physico-Chemistry Initial Microbial Adhesive Interactions- Mechanisms and Methods Microbiology Reviews.pdf. *FEMS Microbiol. Rev.* **2017**, *23*, 179–230.

(61) Oh, Y. J.; Lee, N. R.; Jo, W.; Jung, W. K.; Lim, J. S. Effects of Substrates on Biofilm

Formation Observed by Atomic Force Microscopy. *Ultramicroscopy* **2009**, *109* (8), 874–880. https://doi.org/10.1016/j.ultramic.2009.03.042.

(62) Berne, C.; Ellison, C. K.; Ducret, A.; Brun, Y. V. Bacterial Adhesion at the Single-Cell Level. *Nat. Rev. Microbiol.* **2018**, *16* (10), 616–627. https://doi.org/10.1038/s41579-018-0057-5.

(63) Fletcher, M.; Loeb, G. I. Influence of Substratum Characteristics on the Attachment of a Marine Pseudomonad to Solid Surfaces. *Appl. Environ. Microbiol.* **1979**, *37* (1), 67–72.

(64) Pringle, J. H.; Fletcher, M. Influence of Substratum Wettability on Attachment of Freshwater Bacteria to Solid Surfaces. *Appl. Environ. Microbiol.* **1983**, *45* (3), 811–817.

(65) Mayrhofer, L.; Moras, G.; Mulakaluri, N.; Rajagopalan, S.; Stevens, P. A.; Moseler, M. Fluorine-Terminated Diamond Surfaces as Dense Dipole Lattices: The Electrostatic Origin of Polar Hydrophobicity. *J. Am. Chem. Soc.* **2016**, *138* (12), 4018–4028. https://doi.org/10.1021/jacs.5b04073.

(66) Kondo, T.; Honda, K.; Tryk, D. A.; Fujishima, A. AC Impedance Studies of Anodically Treated Polycrystalline and Homoepitaxial Boron-Doped Diamond Electrodes. *Electrochim. Acta* **2003**, *48* (19), 2739–2748. https://doi.org/10.1016/S0013-4686(03)00391-8.

(67) Rumbo, C.; Tamayo-Ramos, J. A.; Caso, M. F.; Rinaldi, A.; Romero-Santacreu, L.; Quesada, R.; Cuesta-López, S. Colonization of Electrospun Polycaprolactone Fibers by Relevant Pathogenic Bacterial Strains. *ACS Appl. Mater. Interfaces* **2018**, *10* (14), 11467–11473. https://doi.org/10.1021/acsami.7b19440.

(68) Sultana, S. T.; Babauta, J. T.; Beyenal, H. Electrochemical Biofilm Control: A Review.

Biofouling **2015**, *31* (9–10), 745–758. https://doi.org/10.1080/08927014.2015.1105222.

(69) Zhao, S.; Larsson, K. Theoretical Study of the Energetic Stability and Geometry of Terminated and B-Doped Diamond (111) Surfaces. *J. Phys. Chem. C* **2014**, *118* (4), 1944–1957. https://doi.org/10.1021/jp409278x.

Table of Contents Graphic